Hue University Journal of Science: Natural Science
Vol. 132, No. 1D, 87–97, 2023

pISSN 1859-1388
eISSN 2615-9678

Jost function formalism with complex potential

K. Mizuyama[1,2], T. Dieu Thuy[3], D. Quang Tam[3,4]

[1] Institute of Research and Development, Duy Tan University, Da Nang, VietNam
[2] Faculty of Natural Sciences, Duy Tan University, Da Nang, VietNam
[3] Faculty of Physics, University of Education, Hue University, 34 Le Loi Street, Hue, Vietnam
[4] Faculty of Basic Sciences, University of Medicine and Pharmacy, Hue University, Hue, Vietnam

* Correspondence to K. Mizuyama <mizuyamakazuhito@dtu.edu.vn>
(*Received: 15 February 2023; Revised: 22 May 2023; Accepted: 22 May 2023*)

Abstract. The Jost function formalism is extended with use of the complex potential in this paper. We derive the Jost function by taking into account the dual state which is defined by the complex conjugate the complex Hamiltonian. By using the unitarity of the S-matrix which is defined by the Jost function, the optical theorem with the complex potential is also derived. The role of the imaginary part of the complex potential for both the bound states and the scattering states is figured out. The numerical calculation is performed by using the complex Woods-Saxon potential, and some numerical results are demonstrated to confirmed the properties of extended Jost function formalism.

Keywords: nuclear physics, nuclear structure, Jost Function, complex potential

1 Introduction

The optical model has been used to analyze and successfully reproduced the experimental cross section of the nucleon-nucleus (NA) scattering at higher energy region [1]. As is well known, the optical potential is given by the complex potential, and the imaginary part of the optical potential is important for the quantitative reproduction of the experimental data because it has the absorptive effect to the incident nucleon flux on the NA scattering as written in many papers and textbooks. According to the Feshbach projection theory [2], the origin of the complex optical potential is due to the channels coupling at the intermediate states of the NA-scattering. Nevertheless, the optical potential parameters are given phenomenological so as to reproduce the experimental data [3, 4].

Recently, the microscopic optical potential (MOP) based on the particle-vibration coupling (PVC) method has been carried out. The elastic and inelastic cross section of the NA-scattering have successfully reproduced the experimental data without any fitting parameters because the MOP has been calculated by using the effective nucleon-nucleon interaction self-consistently [5, 6, 7, 8]. In the PVC method, the MOP is represented by the Hartree-Fock mean field potential and self-energy function. The self-energy function is given by the complex non-local function which represents the coupling between the incoming nucleon and excitation of that target nucleus. The excitation of the target is calculated by the self-consistent random phase approximation (RPA). The elastic, inelastic and nucleon capture channels are automatically taken into account in the self-energy function as the intermediate states of the NA-scattering. The description of MOP by PVC is consistent with the Feshbach projection theory.

The contribution of the optical potential can be interpreted as the mean contribution from the coupling of many channels at higher incident incident energy of NA scattering. At low energy, the basic shape of the cross section is characterized by the individual contribution of shape resonances. As expected from the R-matrix theory [9, 10, 11] and results and analysis by continuum PVC [5], the channel coupling effect will play crucial role for the production of the sharp peaks of resonances. The absorptive effect of optical potential becomes smaller. This is the fact which can be expected from the absolute value of the reaction cross section (which is defined by the difference of the total and elastic cross section).

The important role of the imaginary part of the complex potential is not only for the nuclear reaction. The role of the complex potential for the nuclear structure has been discussed. In order to analyze the PVC effect on the single particle levels, the experimentally determined spectroscopic factor has been analyzed by comparing with the theoretically calculated level density [12]. It was confirmed that the experimental spectroscopic factors are reasonably well reproduced in both senses; the position of the centroid energies and the fragmentation. This is another aspect of the complex self-energy function (complex optical potential)'s effect.

The Jost function is one of the useful tool to investigate the role of the potential for bound states, resonances and scattering states, because it is possible to calculate all of those states as the poles of the S-matrix on the complex energy/momentum plane directly from the potential. Recently, we extended the Jost function formalism based on the Hartree-Fock-Bogoliubov (HFB) formalism in order to take into account the pairing [13]. This extension of the Jost function is a kind of the extension to the multi-channel system because the HFB is also a kind of two channel system in a broad sense. However, the potential in the Jost function framework is still supposed to be real. Therefore, we shall extend the Jost function framework with the complex potential in this paper.

2 Jost function with the complex potential

When the potential is given by the complex, the hermiticity of the Hamiltonian is broken. As is well-known, the dual Hilbert space which is defined by the complex conjugate of the Hamiltonian H^* exists if the hermiticity of the Hamiltonian is broken. In order to derive the Jost function with the complex potential, it is necessary to take into account the dual space.

2.1 Derivation of the Jost function

In this section, we shall derive the Jost function with the complex potential.

When the Schrodinger equation is given by

$$\left[-\frac{\hbar^2}{2m}\left(\frac{\partial^2}{\partial r^2}-\frac{l(l+1)}{r^2}\right)+U_{lj}(r)\right]\varphi_{lj}(r;k) = \epsilon(k)\varphi_{lj}(r;k), \quad (1)$$

with the complex potential $U_{lj}(r)$, the equation for the dual state is given by

$$\left[-\frac{\hbar^2}{2m}\left(\frac{\partial^2}{\partial r^2}-\frac{l(l+1)}{r^2}\right)+U^*_{lj}(r)\right]\tilde{\varphi}_{lj}(r;k) = \epsilon(k)\tilde{\varphi}_{lj}(r;k), \quad (2)$$

where

$$\epsilon(k)=\frac{\hbar^2k^2}{2m}. \quad (3)$$

pISSN 1859-1388
eISSN 2615-9678

By using the Green's theorem, we can obtain the regular and irregular solutions, $\varphi_{lj}^{(r)}(r;k)$ and $\varphi_{lj}^{(\pm)}(r;k)$ as

$$\varphi_{lj}^{(r)}(r;k) = F_l(kr) + \int_0^\infty dr' g_{FR,l}(r,r';k)U_{lj}(r')\varphi_{lj}^{(r)}(r';k) \quad (4)$$

$$\tilde{\varphi}_{lj}^{(r)}(r;k) = F_l(kr) + \int_0^\infty dr' g_{FR,l}(r,r';k)U_{lj}^*(r')\tilde{\varphi}_{lj}^{(r)}(r';k) \quad (5)$$

$$\varphi_{lj}^{(\pm)}(r;k) = O_l^{(\pm)}(kr) + \int_0^\infty dr' g_{FL,l}(r,r';k)U_{lj}(r')\varphi_{lj}^{(\pm)}(r';k) \quad (6)$$

and

$$\tilde{\varphi}_{lj}^{(\pm)}(r;k) = O_l^{(\pm)}(kr) + \int_0^\infty dr' g_{FL,l}(r,r';k)U_{lj}^*(r')\tilde{\varphi}_{lj}^{(\pm)}(r';k) \quad (7)$$

where $F_l(kr) = rj_l(kr)$ and $O_l^{(\pm)} = rh_l^{(\pm)}(kr)$ with $h_l^{(\pm)}(kr) = j_l(kr) \pm in_l(kr)$, and $g_{FR,l}(r,r';k)$ and $g_{FL,l}(r,r';k)$ are the Green's functions defined by

$$g_{FR,l}(r,r';k) \equiv -\frac{2m}{\hbar^2}\frac{k}{2i}\theta(r-r')r,r' \times \left[h_l^{(-)}(kr)h_l^{(+)}(kr') - h_l^{(-)}(kr')h_l^{(+)}(kr)\right] \quad (8)$$

and

$$g_{FL,l}(r,r';k) \equiv \frac{2m}{\hbar^2}\frac{k}{2i}r,r'\theta(r'-r) \times \left[h_l^{(-)}(kr)h_l^{(+)}(kr') - h_l^{(-)}(kr')h_l^{(+)}(kr)\right]. \quad (9)$$

By taking the limit of $r \to \infty$ in Eqs.(4) and (5), we can obtain

$$\lim_{r\to\infty}\varphi_{lj}^{(r)}(r;k) \to F_l(kr) - \frac{2m}{\hbar^2}\frac{k}{2i}O_l^{(-)}(kr)\int_0^\infty dr' O_l^{(+)}(kr')U_{lj}(r')\varphi_{lj}^{(r)}(r';k) + \frac{2m}{\hbar^2}\frac{k}{2i}O_l^{(+)}(kr)\int_0^\infty dr' O_l^{(-)}(kr')U_{lj}(r')\varphi_{lj}^{(r)}(r';k) \quad (10)$$

and

$$\lim_{r\to\infty}\tilde{\varphi}_{lj}^{(r)}(r;k) = F_l(kr) - \frac{2m}{\hbar^2}\frac{k}{2i}O_l^{(-)}(kr)\int_0^\infty dr' O_l^{(+)}(kr')U_{lj}^*(r')\tilde{\varphi}_{lj}^{(r)}(r';k) + \frac{2m}{\hbar^2}\frac{k}{2i}O_l^{(+)}(kr)\int_0^\infty dr' O_l^{(-)}(kr')U_{lj}^*(r')\tilde{\varphi}_{lj}^{(r)}(r';k). \quad (11)$$

Since the Jost function is defined as a coefficient function to connect the regular and irregular solution as

$$\varphi_{lj}^{(r)}(r;k) = \frac{1}{2}\left[J_{lj}^{(+)}(k)\varphi_{lj}^{(-)}(r;k) + J_{lj}^{(-)}(k)\varphi_{lj}^{(+)}(r;k)\right] \quad (12)$$

and

$$\tilde{\varphi}_{lj}^{(r)}(r;k) = \frac{1}{2}\left[\tilde{J}_{lj}^{(+)}(k)\tilde{\varphi}_{lj}^{(-)}(r;k) + \tilde{J}_{lj}^{(-)}(k)\tilde{\varphi}_{lj}^{(+)}(r;k)\right], \quad (13)$$

we can obtain

$$J_{lj}^{(\pm)}(k) = 1 \mp \frac{2m}{\hbar^2}\frac{k}{i}\int_0^\infty dr' O_l^{(\pm)}(kr')U_{lj}(r')\varphi_{lj}^{(r)}(r';k) \quad (14)$$

and

$$\tilde{J}_{lj}^{(\pm)}(k) = 1 \mp \frac{2m}{\hbar^2}\frac{k}{i}\int_0^\infty dr' O_l^{(\pm)}(kr')U_{lj}^*(r')\tilde{\varphi}_{lj}^{(r)}(r';k). \quad (15)$$

It is rather easy to prove the following expressions of the Jost function:

$$J_{lj}^{(\pm)}(k) = \pm\frac{2m}{\hbar^2}\frac{k}{i}W_{lj}(\varphi_{lj}^{(r)},\varphi_{lj}^{(\pm)};k) \quad (16)$$

and

$$\tilde{J}_{lj}^{(\pm)}(k) = \pm\frac{2m}{\hbar^2}\frac{k}{i}W_{lj}(\tilde{\varphi}_{lj}^{(r)},\tilde{\varphi}_{lj}^{(\pm)};k), \quad (17)$$

where W_{lj} is the Wronskian is defined by

$$W_{lj}(\varphi_{lj}^{(r)},\varphi_{lj}^{(\pm)};k) = \frac{\hbar^2}{2m}\left[\varphi_{lj}^{(r)}(r;k)\frac{\partial\varphi_{lj}^{(\pm)}(r;k)}{\partial r} - \varphi_{lj}^{(\pm)}(r;k)\frac{\partial\varphi_{lj}^{(r)}(r;k)}{\partial r}\right] \quad (18)$$

and

$$W_{lj}(\tilde{\varphi}_{lj}^{(r)}, \tilde{\varphi}_{lj}^{(\pm)}; k)$$
$$= \frac{\hbar^2}{2m}\left[\tilde{\varphi}_{lj}^{(r)}(r;k)\frac{\partial\tilde{\varphi}_{lj}^{(\pm)}(r;k)}{\partial r} - \tilde{\varphi}_{lj}^{(\pm)}(r;k)\frac{\partial\tilde{\varphi}_{lj}^{(r)}(r;k)}{\partial r}\right]. \quad (19)$$

By taking the limit of $r \to 0$ for Eq.(6) and Eq.(7), we can obtain

$$\lim_{r\to 0}\varphi_{lj}^{(\pm)}(r;k)$$
$$\to O_l^{(\pm)}(kr)$$
$$+\frac{2m}{\hbar^2}\frac{k}{2i}O_l^{(-)}(kr)\int_0^\infty dr' O_l^{(+)}(kr')U_{lj}(r')\varphi_{lj}^{(\pm)}(r';k)$$
$$-\frac{2m}{\hbar^2}\frac{k}{2i}O_l^{(+)}(kr)\int_0^\infty dr' O_l^{(-)}(kr')U_{lj}(r')\varphi_{lj}^{(\pm)}(r';k) \quad (20)$$

and

$$\lim_{r\to 0}\tilde{\varphi}_{lj}^{(\pm)}(r;k)$$
$$= O_l^{(\pm)}(kr)$$
$$+\frac{2m}{\hbar^2}\frac{k}{2i}O_l^{(-)}(kr)\int_0^\infty dr' O_l^{(+)}(kr')U_{lj}^*(r')\tilde{\varphi}_{lj}^{(\pm)}(r';k)$$
$$-\frac{2m}{\hbar^2}\frac{k}{2i}O_l^{(+)}(kr)\int_0^\infty dr' O_l^{(-)}(kr')U_{lj}^*(r')\tilde{\varphi}_{lj}^{(\pm)}(r';k) \quad (21)$$

Using Eqs.(16)-(17), Eqs.(18)-(19) and Eqs.(20)-(21), we can obtain

$$J_{lj}^{(\pm)}(k) = 1 \mp \frac{2m}{\hbar^2}\frac{k}{i}\int_0^\infty dr' F_l(kr')U_{lj}(r')\varphi_{lj}^{(\pm)}(r';k) \quad (22)$$

and

$$\tilde{J}_{lj}^{(\pm)}(k) = 1 \mp \frac{2m}{\hbar^2}\frac{k}{i}\int_0^\infty dr' F_l(kr')U_{lj}^*(r')\tilde{\varphi}_{lj}^{(\pm)}(r';k). \quad (23)$$

Thus we obtained the Jost function by three types of expressions for each $J_{lj}^{(\pm)}(k)$ and $\tilde{J}_{lj}^{(\pm)}(k)$ as given by Eqs.(14), (15), (16), (17), (22) and (23).

The Jost functions satisfy the following symmetric properties.

$$J_{lj}^{(\pm)*}(k^*) = \tilde{J}_{lj}^{(\mp)}(k) \quad (24)$$

$$J_{lj}^{(\pm)}(-k) = J_{lj}^{(\mp)}(k) \quad (25)$$

and

$$\tilde{J}_{lj}^{(\pm)}(-k) = \tilde{J}_{lj}^{(\mp)}(k). \quad (26)$$

2.2 Bound state

The boundary condition for a bound state $\epsilon_n = \epsilon(k_n)$ is given by

$$\begin{cases} J_{lj}^{(+)}(k_n) = 0 & for\ \varphi_{nlj} \\ \tilde{J}_{lj}^{(+)}(\tilde{k}_n) = 0 & for\ \tilde{\varphi}_{nlj} \end{cases}. \quad (27)$$

From Eqs.(24)-(26), we can obtain

$$\tilde{J}_{lj}^{(+)}(k) = J_{lj}^{(+)*}(-k^*). \quad (28)$$

Therefore we can find the relation between k_n and $\tilde{k}_n$ as

$$\tilde{k}_n = -k_n^*. \quad (29)$$

The relation between the energy eigen value for the dual state $\epsilon(\tilde{k}_n)$ and $\epsilon(k_n)$ is given by

$$\epsilon(\tilde{k}_n) = \epsilon(-k_n^*) = \epsilon^*(k_n). \quad (30)$$

It is very easy to rove that the orthogonality of the bound state wave function is given by

$$\int_0^\infty dr\tilde{\varphi}_{nlj}^*(r)\varphi_{mlj}(r) = \delta_{nm}. \quad (31)$$

By dividing the potential into two parts, real and imaginary parts as

$$U_{lj} = U_{lj}^r - iU_{lj}^i \quad (32)$$

and applying the two potential formula to the Green's function, we can obtain the Dyson equation

$$G_{lj}^{(\pm)}(r,r';k) = G_{0,lj}^{(\pm)}(r,r';k)$$
$$+\int_0^\infty dr'' G_{0,lj}^{(\pm)}(r,r'';k)(-iU_{lj}^i(r''))G_{lj}^{(\pm)}(r'',r';k) \quad (33)$$

pISSN 1859-1388
eISSN 2615-9678

where $G_{0,lj}^{(\pm)}(r,r';k)$ is the Green's function which satisfies the following equation

$$\left(\epsilon(k)-h_{lj}^{0}(r)\right)G_{0,lj}^{(\pm)}(r,r';k)=\delta(r-r') \quad (34)$$

with

$$h_{lj}^{0}(r)=-\frac{\hbar^2}{2m}\left(\frac{\partial^2}{\partial r^2}-\frac{l(l+1)}{r^2}\right)+U_{lj}^{r}(r).$$

Using the spectral representation of $G_{0,lj}^{(\pm)}(r,r';k)$ and $G_{lj}^{(\pm)}(r,r';k)$ in Eq.(33), we can obtain

$$\epsilon_{nlj}\sim\epsilon_{nlj}^{0}-i\frac{\langle\varphi_{nlj}^{0}|U_{lj}^{i}|\varphi_{nlj}\rangle}{\langle\varphi_{nlj}^{0}|\varphi_{nlj}\rangle}, \quad (35)$$

where φ_{nlj}^{0} is the bound state wave function satisfies $h_{lj}^{0}|\varphi_{nlj}^{0}\rangle=\epsilon_{nlj}^{0}|\varphi_{nlj}^{0}\rangle$.

If the potential is real function ($U_{lj}^{*}\to U_{lj}$), obviously $\tilde{J}_{lj}^{(+)}(k)\to J_{lj}^{(+)}(k)$, $\tilde{k}_n\to k_n$.

However,

$$k_n=-k_n^{*} \quad (36)$$

is required due to Eq.(29). Therefore, we can find that k_n for the real potential becomes pure imaginary, and the energy eigen value becomes real number.

2.3 Scattering state and optical theorem

The scattering wave function $\psi_{lj}^{(+)}(r;k)$ has the asymptotic behavior

$$\lim_{r\to\infty}\psi_{lj}^{(+)}(r;k)\to\frac{1}{2}\left[O_l^{(-)}(kr)+S_{lj}(k)O_l^{(+)}(kr)\right], \quad (37)$$

with the S-matrix $S_{lj}(k)$. The scattering wave function as the dual state of Eq.(37) has the asymptotic behavior

$$\lim_{r\to\infty}\tilde{\psi}_{lj}^{(+)}(r;k)\to\frac{1}{2}\left[O_l^{(-)}(kr)+\tilde{S}_{lj}(k)O_l^{(+)}(kr)\right], \quad (38)$$

with the S-matrix $\tilde{S}_{lj}(k)$. By concerning the asymptotic behavior of Eqs.(4) and (5), we can find that $\psi_{lj}^{(+)}(r;k)$ and $\tilde{\psi}_{lj}^{(+)}(r;k)$ are defined by

$$\psi_{lj}^{(+)}(r;k)=\frac{\varphi_{lj}^{(r)}(r;k)}{J_{lj}^{(+)}(k)} \quad (39)$$

and

$$\tilde{\psi}_{lj}^{(+)}(r;k)=\frac{\tilde{\varphi}_{lj}^{(r)}(r;k)}{\tilde{J}_{lj}^{(+)}(k)}. \quad (40)$$

The S-matrix $S_{lj}(k)$ and $\tilde{S}_{lj}(k)$ are defined by

$$S_{lj}(k)=\frac{J_{lj}^{(-)}(k)}{J_{lj}^{(+)}(k)} \quad (41)$$

$$\tilde{S}_{lj}(k)=\frac{\tilde{J}_{lj}^{(-)}(k)}{\tilde{J}_{lj}^{(+)}(k)}, \quad (42)$$

respectively.

From Eqs.(24)-(26), we can derive the following properties of the S-matrix.

$$S_{lj}^{*}(k^{*})=\tilde{S}_{lj}^{-1}(k) \quad (43)$$

$$\tilde{S}_{lj}^{*}(k^{*})=S_{lj}^{-1}(k), \quad (44)$$

therefore we can obtain

$$S_{lj}^{*}(k^{*})\tilde{S}_{lj}(k)=\tilde{S}_{lj}^{*}(k^{*})S_{lj}(k)=1 \quad (45)$$

The scattering states (continuum) is defined on the real axis of the complex momentum plane. Therefore the Unitarity of the S-matrix in the complex potential system is given by

$$S_{lj}^{*}(k)\tilde{S}_{lj}(k)=\tilde{S}_{lj}^{*}(k)S_{lj}(k)=1 \quad (46)$$

when $k^{*}=k$ (*i.e.* k is real).

The T-matrix is defined by

$$T_{lj}(k)=\frac{i}{2}\left(S_{lj}(k)-1\right) \quad (47)$$

$$=\frac{2mk}{\hbar^2}\int_0^{\infty}drF_l(kr)U_{lj}(r)\psi_{lj}^{(+)}(r;k) \quad (48)$$

and

$$\tilde{T}_{lj}(k)=\frac{i}{2}\left(\tilde{S}_{lj}(k)-1\right) \quad (49)$$

$$= \frac{2mk}{\hbar^2}\int_0^\infty dr F_l(kr)U_{lj}^*(r)\tilde{\psi}_{lj}^{(+)}(r;k). \quad (50)$$

From Eqs.(48) and (50), we can obtain

$$T_{lj}^*(k^*) = S_{lj}^*(k^*)\tilde{T}_{lj}(k) \quad (51)$$

and

$$\tilde{T}_{lj}^*(k^*) = \tilde{S}_{lj}^*(k^*)T_{lj}(k). \quad (52)$$

Eq.(51) can be rewritten as

$$-\frac{1}{2i}\left(\tilde{T}_{lj}(k) - T_{lj}^*(k^*)\right) = T_{lj}^*(k^*)\tilde{T}_{lj}(k). \quad (53)$$

This is the generalized optical theorem.

When the potential is real, $\tilde{T}_{lj}(k) = T_{lj}(k)$. Therefore Eq.(53) becomes

$$-Im\ \ T_{lj}(k) = |T_{lj}(k)|^2 \quad (54)$$

on the real axis of the complex momentum k (*i.e.* $k^* = k$).

The Green's theorem leads the following Lippmann-Schwinger equations

$$\psi_{lj}^{(+)}(r;k) = F_l(kr)$$
$$+\int_0^\infty dr' G_{F,l}^{(+)}(r,r';k)U_{lj}(r')\psi_{lj}^{(+)}(r';k) \quad (55)$$

and

$$\tilde{\psi}_{lj}^{(+)}(r;k) = F_l(kr)$$
$$+\int_0^\infty dr' G_{F,l}^{(+)}(r,r';k)U_{lj}^*(r')\tilde{\psi}_{lj}^{(+)}(r';k). \quad (56)$$

Using the Green's function, which is written in many textbook as the free particle Green's function, defined by:

$$G_{F,l}^{(\pm)}(r,r';k)$$
$$= \mp i\frac{2mk}{\hbar^2}$$
$$\times\left[\theta(r-r')F_l(kr')O_l^{(\pm)}(kr)\right.$$
$$\left.+\theta(r'-r)F_l(kr)O_l^{(\pm)}(kr')\right], \quad (57)$$

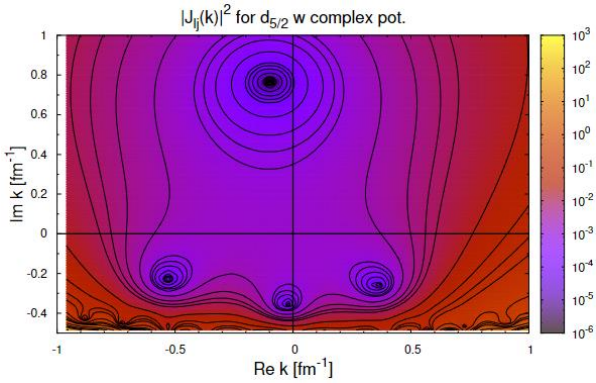

Fig. 1. (Color online) The square of the Jost function $|J_{lj}^{(+)}(k)|^2$ for $d_{5/2}$ which is plotted as a function of the complex momentum k

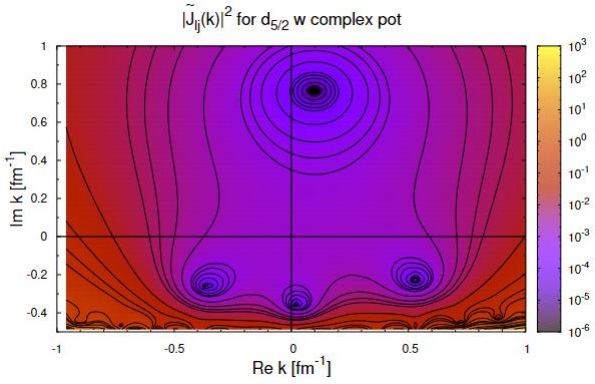

Fig. 2. (Color online) The same as Fig.1 but for $|\tilde{J}_{lj}^{(+)}(k)|^2$

Also, the Green's theorem leads the another types of equations:

$$\psi_{lj}^{(+)}(r;k) = F_l(kr) +$$
$$\int_0^\infty dr' G_{lj}^{(+)}(r,r';k)U_{lj}(r')F_l(kr') \quad (58)$$

and

$$\tilde{\psi}_{lj}^{(+)}(r;k) = F_l(k$$
$$+\int_0^\infty dr' \tilde{G}_{lj}^{(+)}(r,r';k)U_{lj}^*(r')F_l(kr') \quad (59)$$

pISSN 1859-1388
eISSN 2615-9678

using the Green's function defined by

$$G_{lj}^{(\pm)}(r,r';k) = \mp i\frac{2m}{\hbar^2}\frac{k}{J_{lj}^{(\pm)}(k)} \times \left[\theta(r-r')\varphi_{lj}^{(r)}(r';k)\varphi_{lj}^{(\pm)}(r;k) + \theta(r'-r)\varphi_{lj}^{(r)}(r;k)\varphi_{lj}^{(\pm)}(r';k)\right] \quad (60)$$

and

$$\tilde{G}_{lj}^{(\pm)}(r,r';k) = \mp i\frac{2m}{\hbar^2}\frac{k}{\tilde{J}_{lj}^{(\pm)}(k)} \times \left[\theta(r-r')\tilde{\varphi}_{lj}^{(r)}(r';k)\tilde{\varphi}_{lj}^{(\pm)}(r;k) + \theta(r'-r)\tilde{\varphi}_{lj}^{(r)}(r;k)\tilde{\varphi}_{lj}^{(\pm)}(r';k)\right]. \quad (61)$$

$\psi_{lj}^{(-)}(r;k)$ and $\tilde{\psi}_{lj}^{(-)}(r;k)$ are defined by

$$\psi_{lj}^{(-)}(r;k) \equiv \psi_{lj}^{(+)*}(r;k^*) \quad (62)$$

and

$$\tilde{\psi}_{lj}^{(-)}(r;k) \equiv \tilde{\psi}_{lj}^{(+)*}(r;k^*) \quad (63)$$

because $\psi_{lj}^{(-)}(r;k)$ and $\tilde{\psi}_{lj}^{(-)}(r;k)$ are the time-reversal state of $\psi_{lj}^{(+)}(r;k)$ and $\tilde{\psi}_{lj}^{(+)}(r;k)$. Therefore we can obtain

$$\psi_{lj}^{(-)}(r;k) = F_l(kr) + \int_0^\infty dr' G_{F,l}^{(-)}(r,r';k)U_{lj}^*(r')\psi_{lj}^{(-)}(r';k) \quad (64)$$

$$= F_l(kr) + \int_0^\infty dr' \tilde{G}_{lj}^{(-)}(r,r';k)U_{lj}^*(r')F_l(kr') \quad (65)$$

$$= \frac{\tilde{\varphi}_{lj}^{(r)}(r;k)}{J_{lj}^{(-)}(k)} \quad (66)$$

and

$$\tilde{\psi}_{lj}^{(-)}(r;k) = F_l(kr) + \int_0^\infty dr' G_{F,l}^{(-)}(r,r';k)U_{lj}(r')\tilde{\psi}_{lj}^{(-)}(r';k) \quad (67)$$

$$= F_l(kr) + \int_0^\infty dr' G_{lj}^{(-)}(r,r';k)U_{lj}(r')F_l(kr') \quad (68)$$

$$= \frac{\varphi_{lj}^{(r)}(r;k)}{J_{lj}^{(-)}(k)}. \quad (69)$$

From Eqs.(55), (56), (58), (59), (64), (65), (67) and (68), we can derive the following Dyson equations

$$G_{lj}^{(\pm)}(r,r';k) = G_{F,l}^{(\pm)}(r,r';k) + \int_0^\infty dr'' G_{F,l}^{(\pm)}(r,r'';k)U_{lj}(r'')G_{lj}^{(\pm)}(r'',r';k) \quad (70)$$

and

$$\tilde{G}_{lj}^{(\pm)}(r,r';k) = G_{F,l}^{(\pm)}(r,r';k) + \int_0^\infty dr'' G_{F,l}^{(\pm)}(r,r'';k)U_{lj}^*(r'')\tilde{G}_{lj}^{(\pm)}(r'',r';k). \quad (71)$$

Using Eqs.(55), (56) and (71), we can derive

$$\psi_{lj}^{(+)}(r;k) = \tilde{\psi}_{lj}^{(+)}(r;k) + \int_0^\infty dr' \tilde{G}_{lj}^{(+)}(r,r';k)\left(U_{lj}(r') - U_{lj}^*(r')\right)\psi_{lj}^{(+)}(r';k) \quad (72)$$

It should be noted that $\tilde{\psi}_{lj}^{(+)}(r;k) = \psi_{lj}^{(+)}(r;k)$ when the potential is real (*i.e.* $U_{lj} = U_{lj}^*$).

From the limit $r \to \infty$ of Eq.(72), we can obtain

$$\tilde{T}_{lj}(k) = T_{lj}(k) - \frac{2mk}{\hbar^2}\int_0^\infty dr' \tilde{\psi}_{lj}^{(+)}(r';k)\left(U_{lj}(r') - U_{lj}^*(r')\right)\psi_{lj}^{(+)}(r';k). \quad (73)$$

By inserting Eq.(73) into Eq.(53), the generalized optical theorem is rewritten as

$$-Im\ \ T_{lj}(k)$$

$$= |T_{lj}(k)|^2 - \frac{2mk}{\hbar^2}\int_0^\infty dr' |\psi_{lj}^{(+)}(r';k)|^2\ \ Im\ \ U_{lj}(r'), \tag{74}$$

when k is real.

This is the optical theorem with the complex potential. The left hand side of Eq.(74) represents the total cross section. In the right hand side of Eq.(74), the 1st term represents the elastic scattering cross section, the 2nd term represents the difference between the total and elastic cross section. When $Im\ U_{lj}(r)$ is negative, the potential is absorptive because the 2nd term is positive. (The signature of the absorption by potential is given by $\sigma_{tot} > \sigma_{el}$.)

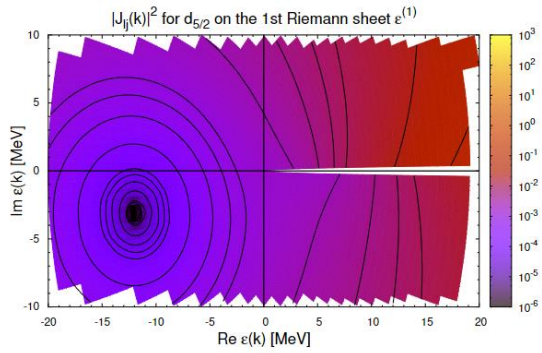

Fig. 3. Figure 3: (Color online) The square of the Jost function $|J_{lj}^{(+)}(k)|^2$ for $d_{5/2}$ which is plotted on the first Riemann sheet $\epsilon^{(1)}$

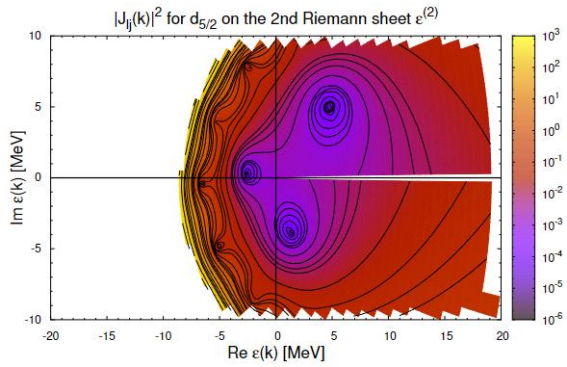

Fig. 4. (Color online) The same as Fig.3 but on the second Riemann sheet $\epsilon^{(2)}$

3 Numerical results

We adopt the complex Woods-Saxon potential which is given by

$$U_{lj}(r) = -\left[V_1 f_{ws}(x_1) + V_2 \frac{1}{a_2 r} g_{ws}(x_2)\ \ l\cdot\ \ \sigma\right]$$

$$-i\left[V_3 f_{ws}(x_3) + V_4 \frac{1}{a_4 r} g_{ws}(x_4)\ \ l\cdot\ \ \sigma\right] \tag{75}$$

$$f_{ws}(x) = \frac{1}{1+e^x},\quad g_{ws}(x) = -\frac{df_{ws}(x)}{dx} \tag{76}$$

$$x_i = (r - R_i)/a_i. \tag{77}$$

$$R_i = \alpha_i A^{\gamma_i} + \beta_i,\quad (i \in 1,\cdots,4) \tag{78}$$

$$l\cdot\ \ \sigma\ = j(j+1) - l(l+1) - \frac{3}{4}. \tag{79}$$

As the original set of the parameters, we adopt

$$A = 24$$

$$V_1 = 51.0\ \ MeV\,,\quad V_2 = 17.0\ \ MeV\ \ fm^2$$

$$V_3 = 5.0\ \ MeV\,,\quad V_4 = 0.0\ \ MeV\ \ fm^2$$

$$a_1 = \cdots = a_4 = 0.67\ \ fm$$

$$\alpha_1 = \cdots = \alpha_4 = 1.27\ \ fm$$

$$\beta_1 = \cdots = \beta_4 = 0.0\ \ fm$$

$$\gamma_1 = \cdots = \gamma_4 = 0.33\ \ fm$$

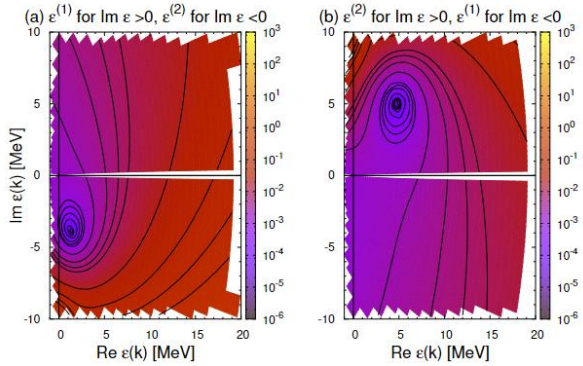

Fig. 5. (Color online) The analytic continuation between the first and second Riemann sheets. In the left panel, the upper-half of Fig.3 and the lower-half of Fig.4 are shown. In the right panel, the upper-half of Fig.4 and the lower-half of Fig.3 are shown

In Figs.1 and 2, the numerical results of $|J_{lj}^{(+)}(k)|^2$ and $|\tilde{J}_{lj}^{(+)}(k)|^2$ for $d_{5/2}$ calculated with the complex Woods-Saxon potential are shown on

pISSN 1859-1388
eISSN 2615-9678

the complex momentum-k plane. Because of the definition of the S-matrix Eqs.(41) and (42), the minimum points which correspond to $|J_{lj}^{(+)}(k)|^2 = 0$ in Fig.1 and $|\tilde{J}_{lj}^{(+)}(k)|^2 = 0$ in Fig.2 represent the poles of $S_{lj}(k)$ and $\tilde{S}_{lj}(k)$, respectively. We can see the symmetric properties between $J_{lj}^{(+)}(k)$ and $\tilde{J}_{lj}^{(+)}(k)$ which are given by Eqs.(24)-(26) in comparison between Fig.1 and Fig.2. It should be noted that the S-matrix poles will be found symmetrically on the Im k axis, and the bound states appear on the Im k axis, if the potential is given by real function.

Since the energy is represented by the momentum as $\epsilon(k) = \frac{\hbar^2 k^2}{2m}$, two kinds of the Riemann sheets of the complex energy, the first and second Riemann sheets ($\epsilon^{(1)}$ and $\epsilon^{(2)}$), are defined by k for Im $k > 0$ and Im $k < 0$, respectively.

In Figs.3 and 4, $|J_{lj}^{(+)}(k)|^2$ for $d_{5/2}$ is represented on $\epsilon^{(1)}$- and $\epsilon^{(2)}$-planes, respectively. Note that Figs.3 and 4 are corresponding to the upper-half and lower-half of the complex-k plane shown in Fig.1, respectively. One can see the discontinuity between the first and fourth quadrant across the branch-cut which is defined by the real axis of the complex energy plane in the positive region in both Figs.3 and 4.

The analytic continuation of $\epsilon^{(1)}$- and $\epsilon^{(2)}$-plane is shown in Fig.5. The first quadrant of Fig.3 is connected with the fourth quadrant of Fig.4, and the first quadrant of Fig.4 is connected with the fourth quadrant of Fig.3. This is due to the regularity of the Jost function on the complex momentum plane.

In Table.1, we show the numerical results for the single particle levels with the real potential and complex potential obtained by searching the zeros of the Jost function on the complex momentum plane. The imaginary part of the single particle levels Im e_n obtained by using the complex potential are given by negative values. This is consistent with the approximated formula given by Eq.(35) since the imaginary part of the potential is given by the negative value in this study. The real part of the single particle levels are slightly shifted to higher energy due to the effect of the imaginary part of the potential.

Table 1. Single particle levels for the bound neutrons for the real potential and complex potential, respectively.

			Real potential ($V_3 = 0$ MeV)		Complex potential ($V_3 = 5.0$ MeV)	
n	l	$2j$	Re e_n	Im e_n	Re e_n	Im e_n
1	0	1	-34.7800	0.0000	-34.7596	-4.3341
1	1	3	-23.5408	0.0000	-23.4992	-3.7736
1	1	1	-19.7961	0.0000	-19.7520	-3.8138
1	2	5	-12.0097	0.0000	-11.9410	-3.1081
2	0	1	-8.6164	0.0000	-8.5116	-2.7687
1	2	3	-5.3174	0.0000	-5.2062	-2.9906
1	3	7	-0.7096	0.0000	-0.5793	-2.2661

4 Conclution

In this study, we extended the Jost function formalism based on the complex potential. Since the Jost function is defined as the coefficient function to connect the regular and irregular solutions of the Schrodinger equation, the Jost function can be derived by finding the relation between the regular and irregular solutions by using the Green's theorem with the proper boundary conditions for each solutions. In the system defined by the Hamiltonian H with the complex potential, two kinds of the Jost function are defined, the Jost function for the system defined by H and the Jost function for the dual system defined by H^*. In order to make sure our derivation, we derived the symmetric properties of the Jost function and confirmed them by the numerical results represented on the complex energy/momentum plane.

As is written in many textbooks, the generalized optical theorem which includes the absorption as the effect of the imaginary part of the complex potential is rather well known. In order to confirm our derivation of the Jost function, firstly we derived the generalized unitarity of the S-matrix by using the Jost function which is calculated by the complex potential. Using the generalized unitarity of the S-matrix, we derived the generalized optical theorem. In order to confirm the effect of the imaginary part of the complex potential to the bound states, we derived an approximated formula which shows the effect of the imaginary part of the potential to the single particle levels by using the Green's function method. And we confirmed that the numerical results for the single particle levels obtained by using the Jost function are consistent with the derived formula.

The results of Table 1 are not qualitatively consistent with the results of the previous cPVC calculation. According to the discussion and results in [12], the complex potential which is calculated as the self-energy function within the PVC has the effect to shift the single particle levels to lower energy, and provides large fragmentation to the single particle levels far from the Fermi level. As shown in [5, 6, 7, 8], the PVC self-energy function works very well as the microscopic optical potential also for the description of the NA-scattering cross section.

For the quantitative reproduction of the experimental data of the NA-scattering, the global optical potential has adopted the complex Woods-Saxon form with the energy dependence. The energy dependence has been given by adjusting the experimental data, but the energy dependence has been given only for the positive energy region, except the Dispersive Optical Potential [14]. In order to obtain the proper interpretation of physics from the analysis of the experimental data using the phenomenological optical potential, the optical potential should be available for both the nuclear structure (single particle levels and their fragmentation and so on) and the nuclear reaction. The Jost function may be a powerful tool to construct such a new type of the optical potential.

According to the Feshbach projection theory [2], the origin of the complex potential is the coupling of channels, and the channel-coupling equation can be reduced to the single channel problem by introducing the complex optical potential. As we showed in this paper, two kinds of the Riemann sheets are defined for two types of the Jost function with the complex potential. On the other hand, the multiple Riemann sheets (more than two, depending on the number of channels) are expected for the channel-coupling equation (The HFB framework is also a kind of the channel-coupling method of two channels in a broad sense, and three types of the Riemann sheets are defined within the HFB framework [13]). Clarifying the relationship between the Riemann surface defined

pISSN 1859-1388
eISSN 2615-9678

by the complex optical potential and the coupled-channel method is also a very interesting subject and one of the directions for future research using the method of Jost functions.

Acknowledgments

This work is funded by Vietnam National Foundation for Science and Technology Development (NAFOSTED) under grant number "103.04-2019.329". D. Quang Tam was funded by the Master, PhD Scholarship Programme of Vingroup Innovation Foundation (VINIF), code VINIF.2022.TS109. D. Quang Tam acknowledges the partial support of Hue University under the Core Research Program, Grant no. NCM.DHH.2018.09.

References

1. Feshbach H, Porter CE, Weisskopf VF. Model for Nuclear Reactions with Neutrons. Physical Review. 1954;96(2):448-64.
2. Feshbach H. Unified theory of nuclear reactions. Annals of Physics. 1958;5(4):357-90.
3. Kunieda S, Chiba S, Shibata K, Ichihara A, SukhovitskĬ ES. Coupled-channels Optical Model Analyses of Nucleon-induced Reactions for Medium and Heavy Nuclei in the Energy Region from 1 keV to 200 MeV. Journal of Nuclear Science and Technology. 2007;44(6):838-52.
4. Perey F, Buck B. A non-local potential model for the scattering of neutrons by nuclei. Nuclear Physics. 1962;32:353-80.
5. Mizuyama K, Ogata K. Self-consistent microscopic description of neutron scattering by ^{16}O based on the continuum particle-vibration coupling method. Physical Review C. 2012;86(4):041603.
6. Mizuyama K, Ogata K. Low-lying excited states of $^{24}\mathrm{O}$ investigated by a self-consistent microscopic description of proton inelastic scattering. Physical Review C. 2014;89(3):034620.
7. Hao TVN, Loc BM, Phuc NH. Low-energy nucleon-nucleus scattering within the energy density functional approach. Physical Review C. 2015;92(1):014605.
8. Blanchon G, Dupuis M, Arellano HF, Vinh Mau N. Microscopic positive-energy potential based on the Gogny interaction. Physical Review C. 2015;91(1):014612.
9. Lane AM, Thomas RG. R-Matrix Theory of Nuclear Reactions. Reviews of Modern Physics. 1958;30(2):257-353.
10. Kapur PL, Peierls RE. The dispersion formula for nuclear reactions. Proc Roy Soc. 1938;166A:277.
11. Wigner EP, Eisenbud L. Higher Angular Momenta and Long Range Interaction in Resonance Reactions. Physical Review. 1947;72(1):29-41.
12. Mizuyama K, Colò G, Vigezzi E. Continuum particle-vibration coupling method in coordinate-space representation for finite nuclei. Physical Review C. 2012;86(3):034318.
13. Mizuyama K, Le NN, Thuy TD, Hao TVN. Jost function formalism based on the Hartree-Fock-Bogoliubov formalism. Physical Review C. 2019;99(5):054607.
14. Atkinson MC, Mahzoon MH, Keim MA, Bordelon BA, Pruitt CD, Charity RJ, et al. Dispersive optical model analysis of $^{208}\mathrm{Pb}$ generating a neutron-skin prediction beyond the mean field. Physical Review C. 2020;101(4):044303.